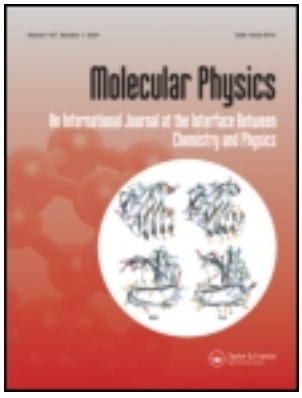

Molecular Physics: An International Journal at the Interface Between Chemistry and Physics
Publication details, including instructions for authors and subscription information:
http://www.tandfonline.com/loi/tmph20

The effects of interaction range, porosity and molecular association on the phase equilibrium of a fluid confined in a disordered porous media

A. Naresh Kumar [a] & Jayant K. Singh [a]
[a] Department of Chemical Engineering, Indian Institute of Technology Kanpur, Kanpur, India-208016
Published online: 20 Nov 2008.

To cite this article: A. Naresh Kumar & Jayant K. Singh (2008) The effects of interaction range, porosity and molecular association on the phase equilibrium of a fluid confined in a disordered porous media, Molecular Physics: An International Journal at the Interface Between Chemistry and Physics, 106:19, 2277-2288, DOI: 10.1080/00268970802418963

To link to this article: http://dx.doi.org/10.1080/00268970802418963

Molecular Physics
Vol. 106, No. 19, 10 October 2008, 2277–2288

RESEARCH ARTICLE

The effects of interaction range, porosity and molecular association on the phase equilibrium of a fluid confined in a disordered porous media

A. Naresh Kumar and Jayant K. Singh*

Department of Chemical Engineering, Indian Institute of Technology Kanpur, Kanpur, India-208016

(*Received 27 May 2008; final version received 18 August 2008*)

Grand-canonical transition-matrix Monte Carlo (GC-TMMC) is employed to analyse the effects of range of interaction, packing fraction and molecular association on phase coexistence properties of square-well (SW) based fluids in disordered pores. The nature of the phase equilibria were studied inside a repulsive disordered porous media with packing fractions, $\eta_m = 0.05$ and 0.10. Three values of the SW attractive well range parameter were studied: $\lambda = 1.5$, 1.75, and 2.0. Coexistence number probability distribution reflects the signature of the disordered structure of the porous matrix. Yet, no multiple fluid–fluid transition was observed. The effect of strength of molecular association on coexistence densities, density profile, saturation pressure, and monomer fraction for the SW based dimerizing fluids inside a repulsive disordered media is reported. Association is found to increase as the packing fraction of the matrix increase. Critical properties of these confined fluids are calculated via a rectilinear diameter approach. Fractional shift in the critical temperature linearly decreases with the increase in the attractive well width for non-associating fluids. The rate of decrease in the critical temperature shift increases with the increase in packing fraction. Associating sites are found to suppress the shift in the critical temperature.

Keywords: Square-well fluids; associating fluids; disordered pores

1. Introduction

Investigation of phase coexistence, adsorption, diffusion and reaction of fluids in disordered porous materials is of much interest from both a scientific and industrial point of view. Improved knowledge of thermophysical properties of fluids confined in narrow pores can provide better solutions to chemical, oil and gas, food and pharmaceutical industries, mixture separation, and as catalysts and their supporters for chemical reactions [1–3]. In general, molecules confined within narrow pores, with pore widths of a few molecular diameters, can exhibit a wide range of physical behaviour. The complex pore geometry and the competition between fluid–wall and fluid–fluid forces can lead to intriguing phase changes.

Recent experimental studies [4–14] of fluids confined in disordered media for example, porous glasses, aerogels, etc., have revealed that the phase behaviour in disordered media is markedly different from that of their bulk systems under the same conditions. Fascinating behaviour of fluids confined in porous media has led to many investigation using theoretical and simulation techniques. The most common pore models studied have simple geometries such as slit pores [15–22] and cylindrical pores [23–29]. However, less work has been done on disorder materials that have complex pore geometries. Among the theoretical work performed on the fluids confined in disordered materials, the random-field Ising model (RFIM) [30] and single-pore model [31–33] were able to produce the spatial inhomogeneity, although such models were unable to provide evidence of phenomena like wetting. On the other hand, the quenched-annealed (QA) system, in which the disordered matrix realization results from the quench of an equilibrium configuration of matrix particles generated in the absence of the fluid particles [34,35], has proven to be more popular model as it is well suited to studies by integral equation theories [36–39] and computer simulations [40–45].

Page and Monson were the first to apply QA model in molecular simulations to study the phase behaviour of methane confined in silica-xerogels [42,46] using grand-canonical Monte Carlo (GCMC). The authors provided evidence for two-phase transitions. The first phase transition, analogous to the bulk liquid–vapour transition, has a narrow coexistence curve with a lower critical density and temperature. On the other hand,

*Corresponding author. Email: jayantks@iitk.ac.in

ISSN 0026–8976 print/ISSN 1362–3028 online

DOI: 10.1080/00268970802418963
http://www.informaworld.com

the second fluid–fluid transition is found to occur at lower temperatures and higher density. The appearance of the second transition, although highly sensitive to the matrix configuration, is attributed to the wetting properties of the fluid in the more confined regions of the adsorbent. Alvarez *et al.* [45] applied GCMC combined with histogram reweighing technique [47] to study the phase equilibria of a single component fluid within a disordered matrix. The authors used a potential model, in which fluid particles interact by means of hard sphere (HS) potential and an attractive Lennard–Jones (LJ) tail. Brennan and Dong [48] used Gibbs ensemble Monte Carlo (GEMC) method and Gibbs–Duhem integration to study the phase equilibria of LJ fluid in random porous media. The authors were successful in providing a good qualitative agreement with the results found by Page and Monson [42,46]. Gordon and Glandt [44] examined the effect of confinement on phase separation of a symmetric immiscible LJ mixture in a disordered solid matrix using GEMC technique. Subsequently, more studies were reported on the phase diagram [49] and adsorption behaviour in disordered media [50].

Considerable effort has been put on the phase diagram of simple fluids; however, further work is required to gain complete insight into the interesting behaviour of complex fluids in disordered matrices. There were a few investigations using integration equation theories, on the structural behaviour of dimerizing fluids in disordered materials [51,52] nonetheless, there is a lack of studies on the phase coexistence behaviour of associating fluids in disordered materials. Molecular simulations, in this area, has focused mainly on LJ fluids and no work until now has been reported on the vapour–liquid phase diagram of square-well (SW) and model associating fluids in disordered media.

In the present study, we examine the vapour–liquid coexistence properties of variable SW fluids in disordered pores. We present the effect of range of attraction on various properties of SW fluids in disordered matrix. We further study the effect of packing fraction on the properties of these fluids. We also present the vapour–liquid phase equilibria, monomer fraction and density distribution for one-site associating fluids in disordered matrix.

The rest of the paper is organized as follows. In the next section we briefly describe the model and methodology used in this work. Section 3 describes the details of simulation conditions used in this study. Section 4 presents the results for different square-well fluids and SW based one-site associating fluids, followed by conclusions in Section 5.

2. Model and methodology

2.1. *Model*

The porous matrix is generated from an equilibrium configuration of a HS fluid using a canonical Monte Carlo simulation [53]. The packing fraction of this matrix is calculated by $n_m = \pi\rho_m\sigma_m^3/6$, where ρ_m and σ_m are the number density and diameter of matrix particles, respectively. These parameters determine the porosity of the generated matrix. The fluid–fluid interaction is described by the SW potential, which constitutes the simplest fluid model including both repulsive and short-range attractive interactions and is given by

$$u_{sw}(r_{ij}) = \begin{cases} \infty, & 0 < r_{ij} < \sigma, \\ -\varepsilon, & \sigma \le r_{ij} < \lambda\sigma, \\ 0, & \lambda\sigma \le r_{ij} \end{cases} \tag{1}$$

where $\lambda\sigma$ is the potential-well diameter, ε is the depth of the well, and σ is the diameter of hard core. The repulsive matrix nature is modelled by hard sphere interaction given by the following expression

$$u_{mf}(r) = \begin{cases} \infty, & r \le \sigma_{mf} \\ 0, & r > \sigma_{mf} \end{cases} \tag{2}$$

where σ_{mf} is the minimum approaching distance between the fluid and matrix particles.

Associating fluids, in this work, are represented by the SW based model [54]. A square well contribution describes the isotropic van der Waals interaction. In real molecules, association occurs when the molecules are in close proximity and association sites are appropriately oriented. These features are represented in the potential model through an additional orientation-dependent square-well contribution. This one-site associating model represents the dimer-forming molecules [55]. Thus the complete potential is

$$u(r_{ij}, \theta_i, \theta_j) = u_{sw}(r_{ij}) + u_{af}(r_{ij}, \theta_i, \theta_j)$$

$$u_{af}(r_{ij}, \theta_i, \theta_j) = \begin{cases} -\varepsilon_{af}, & \text{if } \theta_i < \theta_c \text{ and } \theta_j < \theta_c \\ -\varepsilon, & \text{otherwise} \end{cases} \tag{3}$$

where θ_i and θ_j are angles between the centre-to-centre vector and the direction vectors on the respective atoms i and j, ε_{af} is the well depth of the association cone, $\lambda\sigma$ is the square-well potential diameter, ε is the depth of the isotropic well, and σ is the diameter of the hard core. We adopt units such that ε and σ are unity. In this study, $\theta_c = 27^\circ$, $\lambda = 1.5$ and $r_c = 1.05$. In this work, we have examined the properties of one-site model for association energies, $\varepsilon_{af} = 4.0$ and 7.0.

2.2. *Methodology*

GC-TMMC [56] is used to study the phase coexistence properties of SW and associating fluids. In this approach simulations are conducted in a grand canonical ensemble, in which the chemical potential μ, volume V and temperature T are kept fixed and particle number N and energy U fluctuate. The probability π of observing a microstate s with energy U and particle number N is defined as,

$$\pi_S = \frac{1}{\Xi}\frac{V^{N_S}}{\Lambda^{3N_S}N_S!}\exp[-\beta(U_S - \mu N_S)] \tag{4}$$

where $\beta = 1/k_B T$ is the inverse temperature, Ξ is the grand canonical partition function, and Λ is the de Broglie wavelength. The macrostate probability, $\Pi(N)$, is calculated by summing all the micro-states at a constant number of molecules N. The mathematical formula can be expressed as

$$\Pi(N) = \sum_{N_S=N} \pi_S. \tag{5}$$

To obtain the probability distribution $\Pi(N)$ we employ the transition-matrix Monte Carlo scheme [56], with a N-dependent sampling bias. Multi-canonical sampling [57] is incorporated to ensure adequate sampling of all states with uniform frequency. The probability distribution function is subsequently used to obtain the chemical potential of the coexistence phase through the histogram reweighting method of Ferrenberg and Swendson [47]. This method enables one to shift the probability distribution obtained from a simulation at chemical potential μ_0 to a probability distribution corresponding to a chemical potential μ using the relation

$$\ln \Pi(N;\mu) = \ln \Pi(N;\mu_0) + \beta(\mu - \mu_0)N. \tag{6}$$

We apply Equation (6) to find the coexistence chemical potential that produces a probability distribution $\Pi_c(N)$, where the areas under the vapour and liquid regions are equal. Saturated densities are related to the first moment of the vapour and liquid peaks of the coexistence probability distribution. To calculate the saturation pressure we use the following expression:

$$\beta p V = \ln\left(\sum \Pi_C(N)/\Pi_C(0)\right) - \ln(2). \tag{7}$$

The critical properties are estimated from a least square fit of the scaling law:

$$\rho^l - \rho^v = C_1\left(1 - \frac{T}{T_c}\right)^{\beta_c} \tag{8}$$

where ρ_l and ρ_v are the liquid and vapour densities, respectively, and C_1 and β_c are fitting parameters. The critical temperature estimate from Equation (8) is utilized to get the critical density by using the least square fit to the law of rectilinear diameter [58],

$$\frac{\rho^l + \rho^v}{2} = \rho_c + C_2(T - T_c) \tag{9}$$

where C_2 is a fitting parameter. Critical pressure is calculated using the least square fit to the following expression,

$$\ln P = A + \frac{B}{T} \tag{10}$$

where A and B are constants.

3. Computational details

This work is divided into two parts. In the first part, we use GC-TMMC approach to obtain the coexistence properties for variable square-well fluids in a repulsive disordered media. The trial moves were conducted with frequency 1 : 1.17 : 1.17 for displacement, insertion and deletion, respectively. In the second part, we applied the same technique for one-site associating fluids system along with the implementation of the unbound-bound (UB) algorithm of Wierzchowski and Kofke [59]. The trial moves were performed with frequency 1 : 1 : 2 : 7 for displacement, rotation, bias displacement [59], and insertion–deletion, respectively. Reduced units used in this study are temperature $T^* = KT/\varepsilon$, density $\rho^* = \rho_f \sigma_{ff}^3/(1-\eta_m)$ and pressure $P^* = P\sigma^3/\varepsilon$. Matrix and fluid particles are of same size i.e., $\sigma_{ff} = \sigma_{mm} = \sigma_{mf} = 1$. All the simulations were done in a cubic box of $L^* = 10$. In this work we consider two packing fractions: $\eta_m = 0.05$ and 0.10, which correspond to 95 and 190 matrix particles, respectively. The number of fluid particles varied from 400–850 particles depending on T^* and λ. Three values of potential well diameter were studied: $\lambda = 1.50$, 1.75 and 2.00. Confidence limits were calculated from four independent simulations.

4. Results and discussion

4.1. *Non-associating fluid systems*

We start our discussion with the effect of realization on the phase coexistence properties of a SW fluid. Figure 1 shows the pore size distributions, determined using the algorithm proposed by Bhattacharya and Gubbins [60], for different realizations R1, R2, R3 and R4 created using equilibrium HS simulations at a constant packing fraction, $\eta_m = 0.05$. Pore size

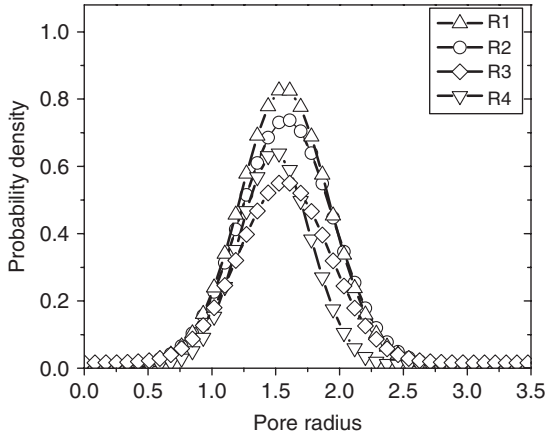

Figure 1. Pore size distributions for matrix realizations R1, R2, R3 and R4 at $\eta_m = 0.05$.

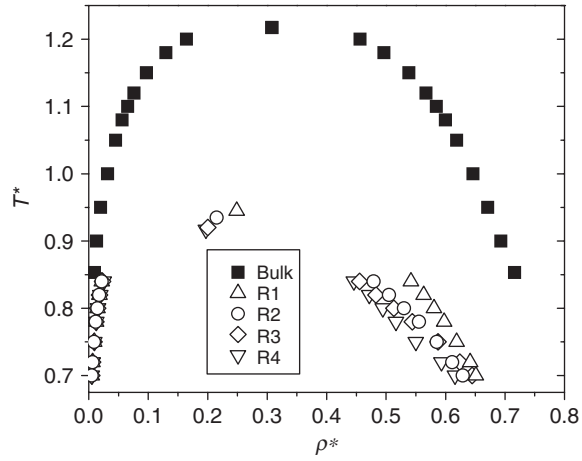

Figure 2. Phase coexistence envelope of a SW fluid in four different realizations of a disordered porous media at $\lambda = 1.50$ and $\eta_m = 0.05$. The squares represent the bulk system and R1, R2, R3 and R4 represents different realizations.

distributions of realizations R1–R4 are similar in nature but with modest differences in the average pore size of the matrix structure. To understand the variation in the phase coexistence properties with realizations, we conducted GC-TMMC simulations for R1–R4. Figure 2 shows the phase coexistence curves for a SW fluid confined in different realizations of a disorder matrix. The results clearly indicate extreme sensitivity of phase coexistence properties to the matrix structure. It is evident that change in the realization may affect saturation densities significantly. For example, at $T^* = 0.7$, the saturated vapour and liquid densities are observed to alter by 5% with the change in realization from R1 to R4 however, corresponding changes at higher temperature,

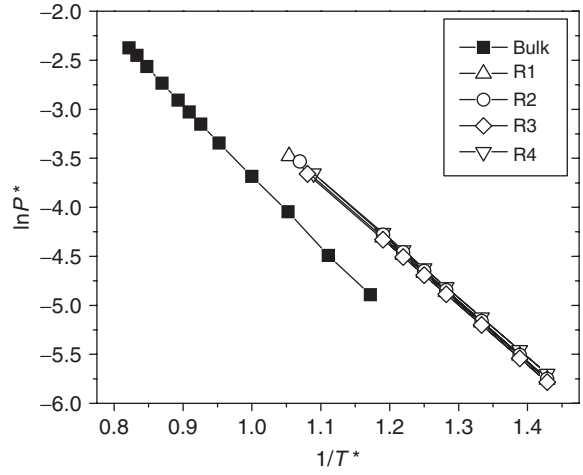

Figure 3. Clausius-Clapeyron plot of a SW fluid of well width: $\lambda = 1.50$, adsorbed in a disordered porous media at $\eta_m = 0.05$. The squares represent the bulk system and R1, R2, R3 and R4 represents different realizations.

$T^* = 0.84$, are 11 and 22% in vapour and liquid densities, respectively; which is significant. Due to the sensitive nature of phase coexistence densities, critical properties also get affected with the change in realization. Critical temperature and density are observed to vary by 3% and 20%, respectively with the change in realization from R1 to R4. Similar behaviour was also observed by Alvarez *et al.* [45] and Brennan and Dong [48] for LJ fluid in HS matrix.

Figure 3 shows the typical Clausius–Clapeyron plot of a SW fluid adsorbed in different realizations. In contrast to the saturation densities, saturation vapor pressure is not sensitive to the matrix realization. However, due to the change in the critical temperature with realization, we obtained slightly different critical pressure for different realizations.

In summary, matrix realizations affect significantly the saturated densities and consequently critical properties of the confined fluid. Rectilinear diameter approach and scaling analysis, as done in this work, is an approximate method to obtain critical properties in disordered media. For accurate values, finite size scaling is most suitable as recently done by Vink *et al.* [61]. However, in this work our focus is to understand, in general, the effects of range of attraction, porosity of the disordered matrix on phase coexistence properties of a confined fluid. Furthermore, the purpose of this study is to compare the general behaviour of the non-associating and associating fluids in a disordered matrix; hence, we postpone a more accurate and deeper investigation in the future. The rest of the study is based on one realization.

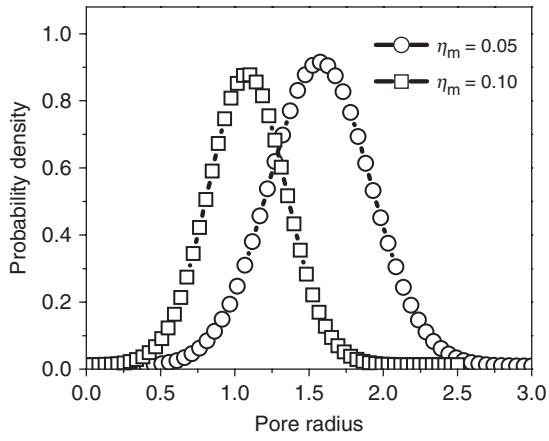

Figure 4. Pore size distributions for the hard sphere matrix at two different packing fractions.

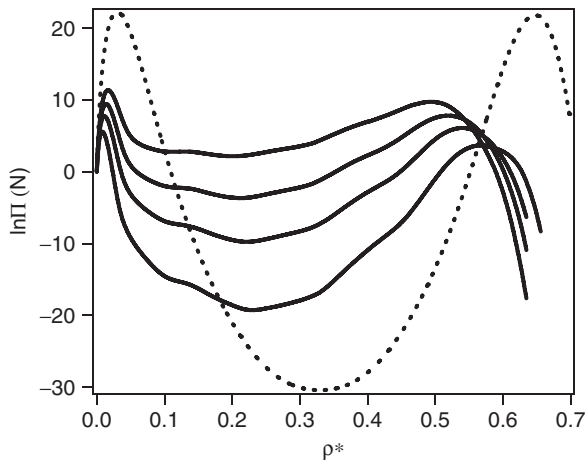

Figure 5. Plot of vapour–liquid coexistence density probability distribution vs. density for a SW fluid with $\lambda = 1.50$ in a repulsive disordered media with $\eta_m = 0.05$. The solid curves from bottom are for the temperatures $T^* = 0.75$, 0.78, 0.80, 0.82, respectively. Bulk probability distribution at $T^* = 1.0$ is shown by the dashed curve.

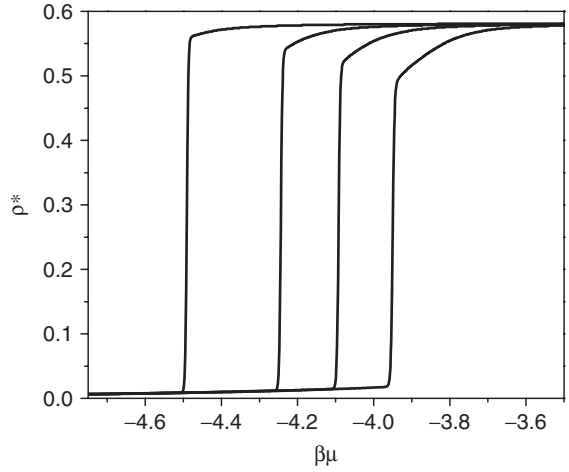

Figure 6. Adsorption isotherm plot of density vs. chemical potential for a SW fluid with $\lambda = 1.50$ in a repulsive disordered media with $\eta_m = 0.05$.The isotherms from left to right are for $T^* = 0.75$, 0.78, 0.80, 0.82, respectively.

Figure 4 shows the pore size distributions of the random matrix at packing fractions, $\eta_m = 0.05$ and 0.10. To our expectation, mean pore size at $\eta_m = 0.10$ is less than that of $\eta_m = 0.05$. In both the cases, we observed a strong Gaussian character, which is observed by other authors for disordered matrix [44,48]. Figure 5 presents the vapour-liquid probability density distribution curve at coexistence, obtained from histogram reweighting technique, for a SW fluid of well-extent $\lambda = 1.5$ confined in a repulsive disordered matrix with packing fraction, $\eta_m = 0.05$. Akin to bulk vapour–liquid probability distribution, we observed two peaks corresponding to vapour and liquid phases in disordered matrix. However, the probability distribution in disordered matrix contains non-regular pattern, which is missing in the bulk probability as shown in the figure. This behaviour is attributed to the random nature of the pores.

In order to understand the adsorption isotherm of SW fluids, histogram reweighting technique is used to generate isotherms with $\Delta\beta\mu = 0.0001$. Figure 6 shows the adsorption isotherm at various temperatures for the system presented in Figure 5. At any particular temperature, with the increase in chemical potential, we observe a single sharp change at coexistence chemical potential. As temperature increases, coexistence chemical potential shifts toward the saturated bulk value [62]. In this work, multiple phase transition was not observed, contrary to Brennan and Dong's work on the LJ fluid in disordered matrix, where multiple fluid–fluid transition were observed though not for all realization of disordered matrix [49].

Figure 7, presents the vapour-liquid phase coexistence envelopes of a SW fluid with $\lambda = 1.50$ adsorbed in HS random matrix of packing fraction: $\eta_m = 0.05$ and 0.10, calculated by GC-TMMC. We observe that the phase coexistence envelope becomes narrower with the increase in packing fraction of the porous media. Akin to the behaviour of square-well fluid in hard-slit pore [22], critical temperature decreases. The decrease is substantial with the increase in packing fraction. A large fraction of the confined molecules experience a reduction in the number of nearest-neighbour molecules, hence lowering of the critical temperature is observed. Critical density also decreases in disordered porous material and it continues to decrease, though relatively less, with the increase

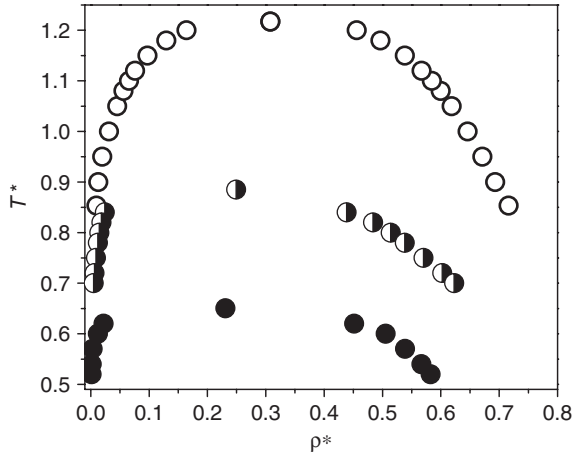

Figure 7. Phase coexistence envelope of a SW fluid with $\lambda = 1.50$ in disordered porous media. The open circles represent the bulk system. The half filled and completely filled circles represent a confined system with $\eta_m = 0.05$ and 0.10, respectively. Statistical error is smaller than the symbol size.

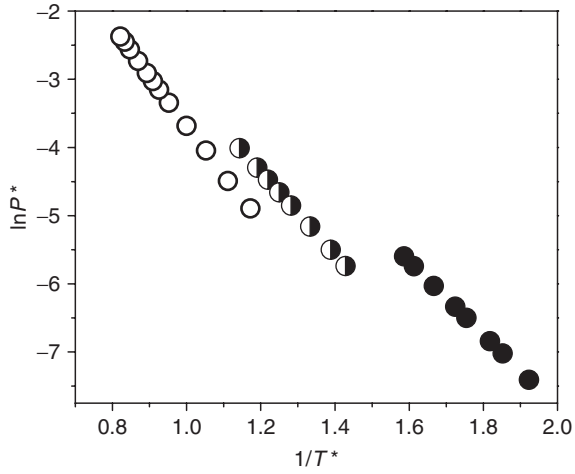

Figure 8. Saturation vapour pressures of SW fluid for $\lambda = 1.50$ in disordered porous media. The open circles represent the bulk system. The half filled and completely filled circles represent a confined system with $\eta_m = 0.05$ and 0.10, respectively. Statistical error is smaller than the symbol size.

in packing fraction. Similar behaviour was observed for LJ fluids in disordered matrix [42,46,48].

Figure 8 presents the saturated vapour pressure of a SW fluid of $\lambda = 1.5$ in repulsive disordered matrix of packing fraction, $\eta_m = 0.05$ and 0.10. The saturation pressures under confinement are observed to be higher than the bulk saturation pressures. Such behaviour was also observed for SW fluids under slit pore [22] and it was found that decrease in the pore size increases the saturation pressure. With the increase in packing fraction, in disordered matrix, average pore size reduces (see Figure 4) and effectively saturation pressure is increased. In addition, it is observed that in presence of confinement, slope of the ln (P) vs $1/T$ plot decreases compared with that of the bulk. Though the decrease in the slope is not dramatic, still it suggests that the enthalpy of vaporization decreases under confinement. This data is reported in Table 1 along with higher attractive well-range: $\lambda = 1.7$ and 2.0. Similar phenomena are observed in the coexistence properties for higher range of attractive well width.

Shift in critical temperature, T_C, in porous material can have interesting relationship with the pore width as studied by few authors for the case of slit-pore [15,63] however, such form of observation may not hold in disordered pores because of its inherent irregular pore structures. In this direction, we have performed simple analysis of shift in critical temperature of fluid confined in the disordered media against the attractive well width and packing fraction. Fractional shift in critical temperature is expressed as $\Delta T_c/T_{c,b} = (T_{c,b} - T_{c,d})/T_{c,b}$, where $T_{c,b}$ is the critical temperature of the bulk fluid and $T_{c,d}$ is the critical temperature of the fluid confined in disordered porous material. Critical properties in this work were obtained using least square fit and rectilinear diameter approach as discussed in Section 2. Table 2 lists the critical properties of variable SW fluids in a repulsive disordered media. Figure 9 shows the fractional shift in the critical temperature for various attractive well-ranges for two packing fractions. Shift in critical temperature is higher at lower well width and reduces with the increase in the attractive well width. This behaviour is due to the greater decrease in the nearest-neighbour molecules at lower well width in the presence of matrix particles. The effect is pronounced at higher packing fraction. Though, the fractional shift in T_C is much higher at $\eta_m = 0.10$; however, the shift in T_C decreases with well width at a much higher rate compared to the case of $\eta_m = 0.05$. Similar behaviour is observed for critical pressure (figure not shown).

Pore structure, in the form of pore size distribution, can change with realization of hard sphere matrix as seen by various authors [1]. Due to the variation in the pore size across the simulation box, we expect to obtain variation in the density of the coexistence phases as also visible from the uneven probability density distribution curve shown in Figure 5. Figure 10(a) and (b) present the local-density profiles of confined SW fluid in liquid and vapour phases, respectively, across the length of the simulation cell for two different temperatures. We clearly observe in both figures that the local-densities fluctuate

Table 1. Vapour–liquid coexistence data of square well fluids with variable potential range ($\lambda = 1.5, 1.75, 2.0$) in disordered matrix of packing fraction, $\eta_m = 0.05$ and 0.10. Subscripts v and l represents vapour and liquid, respectively. The numbers in the brackets are the errors in the last significant digit. The errors are not indicated where the error is an order of magnitude smaller than the last significant digit.

	T^*	ρ_v^*	ρ_l^*	P^*
$\eta_m = 0.05$				
$\lambda = 1.5$	0.84	0.0242	0.4385(4)	0.0136
	0.82	0.0184	0.4839(12)	0.0114
	0.80	0.0150	0.5141(1)	0.0095
	0.78	0.0123	0.5382(1)	0.0078
	0.75	0.0091	0.5704(6)	0.0057
	0.72	0.0066	0.6024(3)	0.0041
	0.70	0.0052	0.6230(5)	0.0032
$\lambda = 1.75$	1.25	0.0292	0.4297(8)	0.0248
	1.22	0.0238	0.4606(1)	0.0211
	1.20	0.0210	0.4781(3)	0.0189
	1.18	0.0186	0.4961(7)	0.0154
	1.15	0.0154	0.5213(8)	0.0140
	1.10	0.0112	0.5593(13)	0.0101
$\lambda = 2.00$	2.02	0.0592	0.4231(4)	0.0665
	2.00	0.0519	0.4448(3)	0.0623
	1.98	0.0465	0.4657(6)	0.0583
	1.95	0.0403	0.493(1)	0.0525
	1.90	0.0323	0.5358(3)	0.0439
	1.85	0.0262	0.5750(9)	0.0363
	1.80	0.0211	0.6111(7)	0.0296
$\eta_m = 0.10$				
$\lambda = 1.5$	0.62	0.0089(13)	0.4517(22)	0.0032
	0.60	0.0052	0.5055(13)	0.0024
	0.58	0.0038	0.5295(8)	0.0018
	0.55	0.0023	0.5564(8)	0.0011
	0.54	0.0020	0.5667(5)	0.0009
	0.52	0.0014	0.5838(4)	0.0006
$\lambda = 1.75$	1.00	0.0258	0.4017(6)	0.0131(1)
	0.95	0.0132	0.4739(5)	0.0089
	0.90	0.0083	0.5226(8)	0.0058
	0.85	0.0051	0.568(1)	0.0035
	0.82	0.0038	0.5957(5)	0.0026
	0.80	0.0030	0.6108(6)	0.0020
$\lambda = 2.00$	1.67	0.0520(1)	0.4544(4)	0.0444
	1.65	0.0438(1)	0.4806(6)	0.0404
	1.62	0.0352(1)	0.5136(1)	0.0350
	1.60	0.0309	0.5340(10)	0.0317
	1.58	0.0272(1)	0.5547(8)	0.0287
	1.55	0.0227	0.5816(16)	0.0245

significantly around their average values. This inhomogeneity within the stable phases is due to the presence of intricate pore structures. The fluctuations are much staggering in liquid phase than in vapour phase. However, in both phases similar signature of variation in the density profile is being observed,

Table 2. Vapour-liquid critical properties of variable square well fluid inside a random porous media estimated from grand-canonical transition-matrix Monte Carlo and rectilinear diameter approach. Numbers in the parenthesis indicate 67% confidence limits of the last digits of the reported value.

System	T_c^*	ρ_c^*	P_c^*
(At $\lambda = 1.50$)			
Bulk	1.2172(7)	0.3079(2)	0.0931(2)
$\eta_m = 0.05$	0.8852(7)	0.2492(9)	0.0181(3)
$\eta_m = 0.10$	0.6505(4)	0.2308(11)	0.0037(11)
(At $\lambda = 1.75$)			
Bulk	1.809(2)	0.2653(1)	0.1263(1)
$\eta_m = 0.05$	1.3519(8)	0.2049(7)	0.03732(2)
$\eta_m = 0.10$	1.0662(3)	0.1905(1)	0.0209(6)
(At $\lambda = 2.00$)			
Bulk	2.7644(1)	0.251(26)	0.1975(43)
$\eta_m = 0.05$	2.1141(3)	0.2214(4)	0.0892(4)
$\eta_m = 0.10$	1.7512(8)	0.2082(13)	0.0631(3)

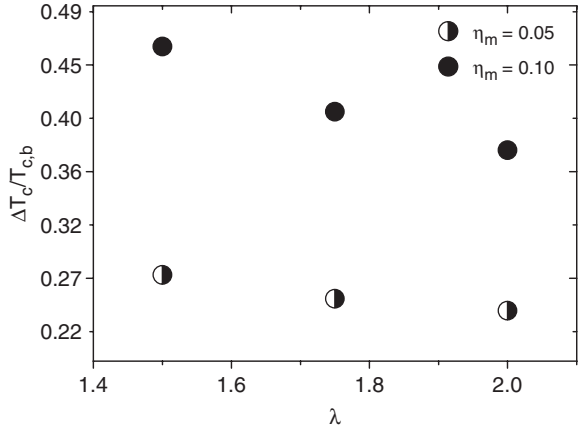

Figure 9. Plot of critical temperature shift in disordered matrix as a function of potential range (λ) for different packing fraction of the matrix.

which is attributed to the random matrix. Such behaviour was also noticed by Brennan and Dong for LJ fluids [48]. This nature of the fluids in disordered porous media is also visible in a typical snapshot, taken in a canonical MC simulation of two phase SW fluid confined in a disordered matrix, as shown in Figure 11.

One of the main objectives of this work was to investigate the effect of associating sites on the phase coexistence behaviour of the fluids in disordered materials. In this direction, we examine the effect of packing fraction of the HS disordered matrix on the properties of one-site associating fluid model and the results are presented in the next sub-section.

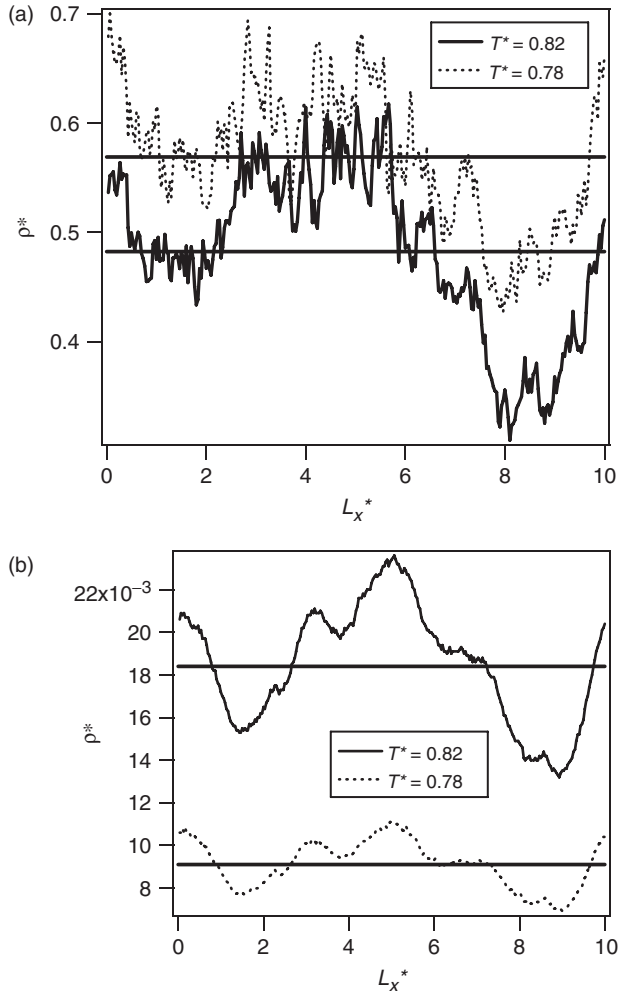

Figure 10. (a) Liquid density profile and (b) vapour density profile of a SW fluid with $\lambda = 1.50$ in a disordered pore of packing fraction, $\eta_m = 0.05$, at two temperatures. The solid straight line represents the average value at that particular temperature. The abscissa is the reduced length of the x-axis of the simulation box.

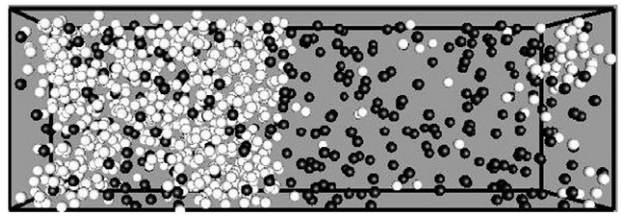

Figure 11. Snapshot of the vapour–liquid configuration of a SW fluid with $\lambda = 1.50$ in a disordered porous media of $\eta_m = 0.05$, at $T^* = 0.80$, from NVT simulation. The black and the white spheres represent matrix and fluid particles, respectively.

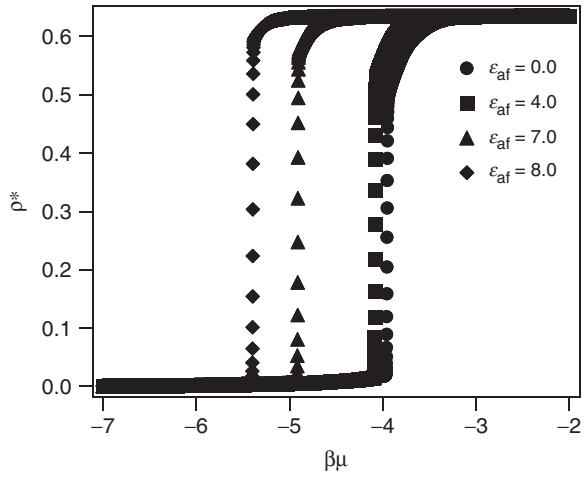

Figure 12. Adsorption isotherm plot of density vs. chemical potential for ASW fluids in a repulsive disordered media of packing fraction, $\eta_m = 0.05$ at $T^* = 0.82$. The isotherms from left to right are for $\varepsilon_{af} = 8.0$, 7.0, 4.0, 0.0, respectively.

4.2. *One-site associating fluid systems*

Figure 12 presents the adsorption isotherms of one-site associating square-well (ASW) fluid for different association energies, ε_{af}, at $T^* = 0.82$ and $\eta_m = 0.05$ using the histogram reweighing technique with $\Delta\beta\mu = 0.0001$. Coexistence chemical potential is found to decrease as the strength of association increases. The probability distribution (figure not shown) obtained using the histogram reweighting technique shows a distinct signature of disorder in the system similar to Figure 5 of non-associating system. However, we did not notice any multiple phase transitions in the adsorption isotherms.

Figure 13 shows the temperature–density coexistence envelope of ASW fluids in a repulsive disordered media with $\eta_m = 0.05$ and 0.10 at $\lambda = 1.50$ for association strength of $\varepsilon_{af} = 4.0$ and 7.0. Similar to the behaviour of bulk associating fluids [54], the general effect of association, irrespective of the type of medium, is to increase the liquid density and to decrease the vapour density. For the liquid the density increase results from the promotion of more compact arrangements of the molecules; for the vapour the decrease in density results from a lowering of vapour pressure with increasing association. As a result of the changes in the density of coexistence liquid and vapour phases, critical temperature increases. This outcome is observed in bulk and as well as in disordered matrix. Figure 14 presents the fraction shift in critical temperature, $\Delta T_c/T_{c,b}$, as a function of association strength and packing fraction. The fractional shift in critical temperature linearly decreases with the increase in the associating strength. This behaviour is analogous to that of non-association fluid (see Figure 9)

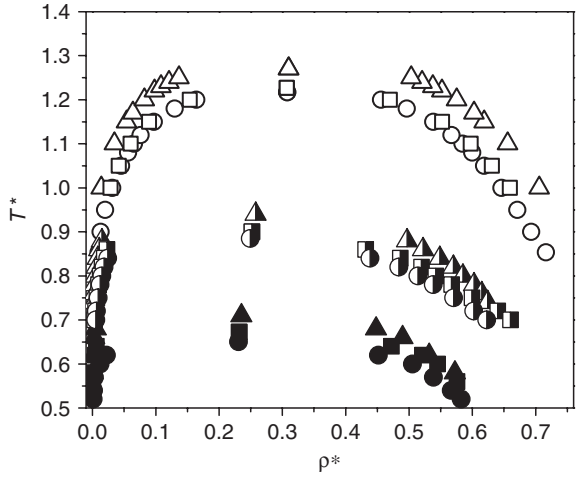

Figure 13. Temperature–density vapour–liquid coexistence envelope of one-site square-well based associating fluids in repulsive disordered media. Circles indicate a system at $\varepsilon_{af}=0.0$ and the squares and triangles represent systems at $\varepsilon_{af}=4.0$ and 7.0, respectively. Open symbols, half filled symbols and completely fill symbols represent disordered matrix with packing fraction, $\eta_m=0.0$, 0.05 and 0.10, respectively. Statistical error is smaller than the symbol size.

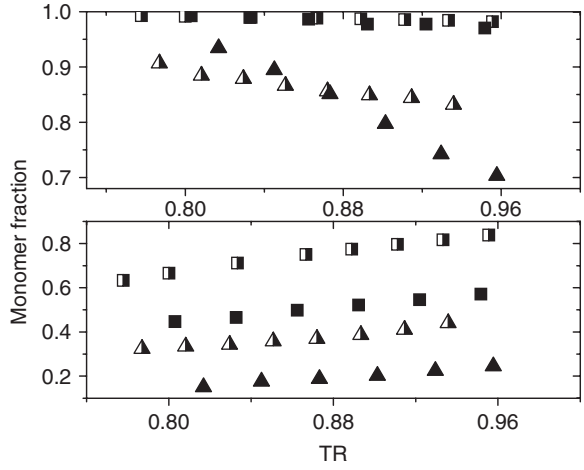

Figure 15. Monomer fraction vs reduced temperature for one-site ASW fluids in repulsive disordered materials. Upper plot represent the vapour phase and lower one is for the liquid phase. Rectangles and triangles represents the associating system at $\varepsilon_{af}=4.0$ and 7.0, respectively. Half filled and completely filled symbols represents a confined system with $\eta_m=0.05$ and 0.10, respectively. Statistical error is smaller than the symbol size.

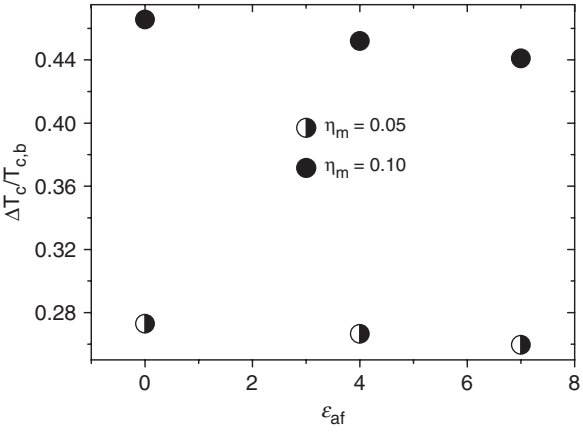

Figure 14. Plot of shift in critical temperature of ASW in disordered matrix of packing fraction, $\eta_m=0.05$ and 0.10, as a function of association strengths.

with attractive well-range taking the role of generating extra energies for molecules, which is done by the associating sites for ASW fluids. The higher association strength tend to suppress the fractional shift in critical temperature due to the tendency of associating fluids to form bonded structure leading to higher liquid density and lower vapour density. This behaviour, in effect, increases the critical temperature.

To substantiate our analysis on the suppression of the shift in the critical temperature in disordered matrix, we examine the change in the monomer fraction in liquid and vapour phases with increase in association strength at different temperatures. Figure 15 presents the monomer fraction against the reduced temperature, $T_R=T^*/T^*_C$. We observe, in general, a decrease in the monomer fraction in vapour phase and an increase in the liquid phase with the increase in temperature for all the packing fraction studied in this work. This behaviour is similar to that of the bulk associating fluid [54]. However, the rate at which monomer fraction drops with temperature substantially increases for associating fluid with $\varepsilon_{af}=7.0$ confined in HS matrix of $\eta_m=0.1$. The difference between vapour and liquid monomer fraction at any particular strength of association decrease with the increase in temperature and finally becomes negligible at the critical temperature. We observe a significant change in the monomer fraction of molecules, particularly at higher association strength, in the presence of disordered matrix. With disordered pores in nature, associating molecules stay closer in bonded form in the local volume available to them in the pores. This behaviour is more pronounced at higher association. Increase in porosity further enhances the association of molecules in both the phases. Association tend to lower the vapour pressure as observed in the bulk fluid [54]. To verify the observation, we studied the variation of saturation pressure of associating fluids as a function of inverse of the reduced temperature, T_R, which is presented in Figure 16. The general behaviour is analogous to that of non-association fluids in

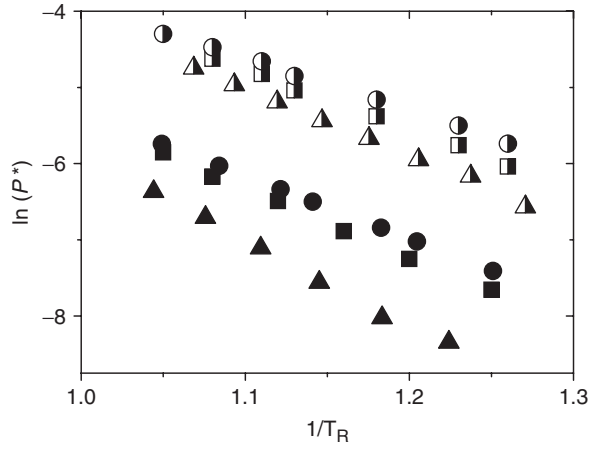

Figure 16. Saturation vapour pressures of ASW fluid in disordered porous media for variable associating strengths. Circle, rectangle and triangle represent the association strength $\varepsilon_{af}=0.0$, 4.0 and 7.0, respectively. Half filled and completely filled symbols represents a confined system with $\eta_m=0.05$ and 0.10, respectively. Statistical error is smaller than the symbol size.

disordered matrix with the variation of packing fraction (see Figure 8). However, for associating fluid, the tendency of molecules to be in the dimer state and the presence of random pores mutually augments the reduction of vapour pressure. This is evident for system at $\varepsilon_{af}=7.0$ and $\eta_m=0.1$, where vapour pressure is substantially less than that of system at $\varepsilon_{af}=4.0$ and $\eta_m=0.1$. The corresponding change in vapour pressure is considerably less at lower packing fraction, $\eta_m=0.05$.

Figure 17(a) and (b) shows the local density profiles of a confined one-site ASW fluid in liquid and vapour phases, respectively from GC-TMMC simulations. We clearly observe in the figures that the local-densities are fluctuating to a significant value. This observation is parallel to the density profile for non-associating fluids as seen in Figure 10. Local-densities in interior pores retain the characteristics of the pore structure for different associating strength studied in this work.

It would be of fundamental interest to obtain interfacial properties of these fluids in disordered matrix. Successful methods like finite size scaling along with Binder's formalism [64] may not be useful, as seen in our preliminary investigation, because of the constraints of maintaining the constant realization for different box sizes. This can be overcome by using a diffusion-limited cluster–cluster aggregation technique, for example, to create the disordered material as recently used by De Grandis *et al.* [65] for silica aerogels. Thorough investigation of interfacial properties of fluid in disordered pores is reserved for future study.

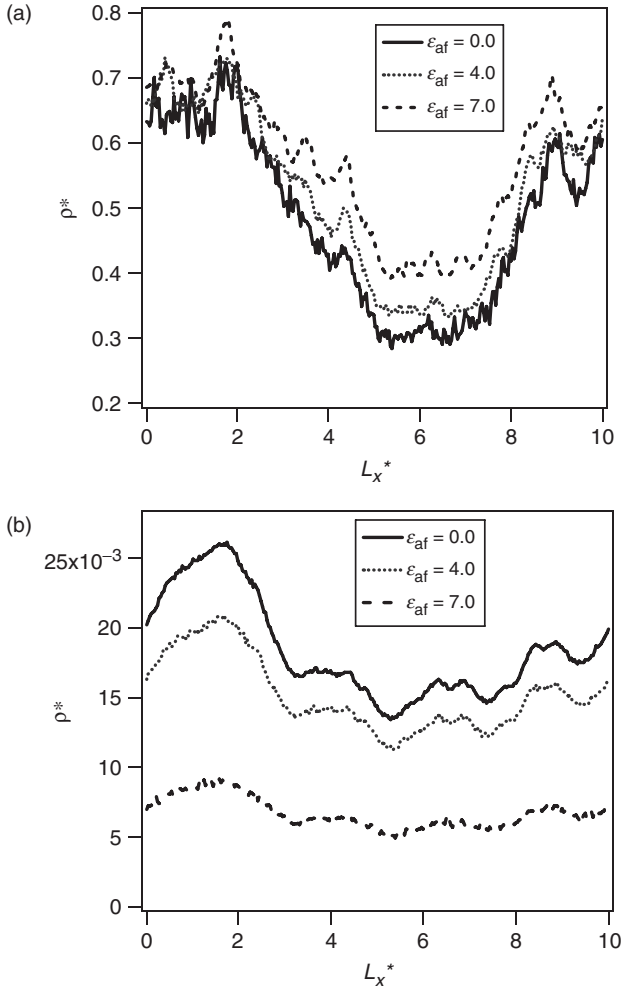

Figure 17. (a) Liquid density profile and (b) vapour density profile of associating SW fluid in a disordered pore with $\eta_m=0.05$ and $T^*=0.82$. The abscissa is the reduced length of the x-axis of the simulation box. Legend indicates values of association strength, ε_{af}.

5. Conclusions

We have investigated the phase behaviour of SW fluids and one-site associating fluids confined in a repulsive disordered matrix. The GC-TMMC technique is demonstrated for the evaluation of the phase equilibria of fluids confined in disordered media. The key features of the confinement effect on SW based fluids are in good qualitative agreement with those in the literature. The phase coexistence envelope of SW fluids of variable interaction range is significantly narrowed in random porous media. The fractional shift in critical temperature and pressure linearly reduces with the increase in the well-extent. This behaviour is intact for higher packing fraction. We further implemented UB algorithm to study the effect of strength of association on the phase coexistence properties of

a model dimerizing fluid in a confined system. The effect of association is to decrease the vapour density and increase the liquid density, while raising the critical temperature. This behaviour remains the same in disordered pores albeit the confinement in the form of hard-disordered matrix invariably narrows the phase envelope and decreases the critical temperature and critical density. We also noticed that disordered pores facilitate more bonded structures, i.e. confinement in the form of hard-disordered pores led to the reduction in monomer fraction in the liquid and vapour phases. Association among molecules is higher in high-packing fraction matrix and vapour pressure diminishes with higher packing fraction. Density profiles of these fluids contain the signature of microstructure of matrix realization. The signature of randomness in the profiles is found to be insensitive to the association strength of the molecules.

Acknowledgements

We wish to thank Dr. Sang Kyu Kwak for helpful conversation. This work was supported by the Department of Science and Technology (Grant No. SR/S3/CE10/2006) and Department of Atomic Energy, Govt. of India (Grant No. 2006/20/36/05-BRNS).

References

[1] L.D. Gelb, K.E. Gubbins, R. Radhakrishnan, *et al.*, Rep. Prog. Phys. **62**, 1573 (1999).
[2] K.R. Matranga, A.L. Myers, and E.D. Glandt, Chem. Eng. Sci. **47**, 1569 (1992).
[3] S. Altwasser, C. Welker, Y. Traa, *et al.*, Microporous Mesoporous Mater. **83**, 345 (2005).
[4] B.J. Frisken and D.S. Cannell, Phys. Rev. Lett. **69**, 632 (1992).
[5] B.J. Frisken, F. Ferri, and D.S. Cannell, Phys. Rev. Lett. **66**, 2754 (1991).
[6] B.J. Frisken, F. Ferri, and D.S. Cannell, Phys. Rev. E **51**, 5922 (1995).
[7] A.P.Y. Wong and M.H.W. Chan, Phys. Rev. Lett. **65**, 2567 (1990).
[8] A.P.Y. Wong, S.B. Kim, W.I. Goldburg, *et al.*, Phys. Rev. Lett. **70**, 954 (1993).
[9] S.B. Kim, J. Ma, and M.H.W. Chan, Phys. Rev. Lett. **71**, 2268 (1993).
[10] Z. Zhuang, A.G. Casielles, and D.S. Cannell, Phys. Rev. Lett. **77**, 2969 (1996).
[11] S.B. Dierker and P. Wiltzius, Phys. Rev. Lett. **58**, 1865 (1987).
[12] S.B. Dierker and P. Wiltzius, Phys. Rev. Lett. **66**, 1185 (1991).
[13] M.Y. Lin, S.K. Sinha, J.M. Drake, *et al.*, Phys. Rev. Lett. **72**, 2207 (1994).
[14] S. Lacelle, L. Tremblay, Y. Bussière, *et al.*, Phys. Rev. Lett. **74**, 5228 (1995).
[15] R. Evans, J. Phys. Condens. Matter. **2**, 8989 (1990).
[16] C.M. Lastoskie, K.E. Gubbins, and N. Quirke, Langmuir **9**, 2693 (1993).
[17] S. Jiang, C.L. Rhykerd, and K.E. Gubbins, Mol. Phys. **79**, 373 (1993).
[18] R.F. Cracknell, D. Nicholson, S.R. Tennison, *et al.*, Adsorption **2**, 193 (1996).
[19] P.B. Balbuena and K.E. Gubbins, Langmuir **9**, 1801 (1993).
[20] U. Marini Bettolo Marconi and F. Van Swol, Phys. Rev. A **39**, 4109 (1989).
[21] M. Schoen and D.J. Diestler, J. Chem. Phys. **109**, 5596 (1998).
[22] J.K. Singh and S.K. Kwak, J. Chem. Phys. **126**, 024702 (2007).
[23] G.S. Heffelfinger, F. Van Swol, and K.E. Gubbins, Mol. Phys. **61**, 1381 (1987).
[24] B.K. Peterson and K.E. Gubbins, Mol. Phys. **62**, 215 (1987).
[25] B.K. Peterson, K.E. Gubbins, G.S. Heffelfinger, *et al.*, J. Chem. Phys. **88**, 6487 (1988).
[26] R. Radhakrishnan and K.E. Gubbins, Phys. Rev. Lett. **79**, 2847 (1997).
[27] E.V. Votyakov, K. Tovbin Yu, J.M.D. MacElroy, *et al.*, Langmuir **15**, 5713 (1999).
[28] M.W. Maddox and K.E. Gubbins, J. Chem. Phys. **107**, 9659 (1997).
[29] R. Evans, U. Marini Bettolo Marconi, and P. Tarazona, J. Chem. Soc. Faraday Trans. **2**, 1763 (1986).
[30] F. Brochard and P.G. de Gennes, J. Phys. (France) Lett. **44**, 785 (1983).
[31] A.J. Liu, D.J. Durian, E. Herbolzheimer, *et al.*, Phys. Rev. Lett. **65**, 1897 (1990).
[32] A.J. Liu and G.S. Grest, Phys. Rev. A **44**, R7894 (1991).
[33] J.P. Donley and A.J. Liu, Phys. Rev. E **55**, 539 (1997).
[34] W.G. Madden and E.D. Glandt, J. Stat. Phys. **51**, 537 (1988).
[35] W.G. Madden, J. Chem. Phys. **96**, 5422 (1992).
[36] E. Kierlik, M.L. Rosinberg, G. Tarjus, *et al.*, J. Phys.: Condens. Matter **8**, 9621 (1996).
[37] E. Kierlik, M.L. Rosinberg, G. Tarjus, *et al.*, J. Chem. Phys. **106**, 264 (1997).
[38] V. Krakoviack, E. Kierlik, M.L. Rosinberg, *et al.*, J. Chem. Phys. **115**, 11289 (2001).
[39] M. Cieplak, A. Maritan, M.R. Swift, *et al.*, Phys. Rev. E **66**, 056124 (2002).
[40] E. Lomba, J.A. Given, G. Stell, *et al.*, Phys. Rev. E **48**, 233 (1993).
[41] A. Meroni, D. Levesque, and J.J. Weis, J. Chem. Phys. **105**, 1101 (1996).
[42] K.S. Page and P.A. Monson, Phys. Rev. E **54**, R29 (1996).
[43] A. Trokhymchuk and S. Sokolowski, J. Chem. Phys. **109**, 5044 (1998).
[44] P.A. Gordon and E.D. Glandt, J. Chem. Phys. **105**, 10 (1996).

[45] M. Alvarez, D. Levesque, and J.J. Weis, Phys. Rev. E **60**, 5495 (1999).
[46] K.S. Page and P.A. Monson, Phys. Rev. E **54**, 6557 (1996).
[47] A.M. Ferrenberg and R.H. Swendsen, Phys. Rev. Lett. **61**, 2635 (1988).
[48] J.K. Brennan and W. Dong, J. Chem. Phys. **116**, 8948 (2002).
[49] J.K. Brennan and W. Dong, Phys. Rev. E **67**, 031503 (2003).
[50] J.K. Brennan, K.T. Thomson, and K.E. Gubbins, Langmuir **18**, 5438 (2002).
[51] D. Henderson, A. Patrykiejew, O. Pizio, *et al*., Physica A **233**, 67 (1996).
[52] P. Padilla, P. Pazio, A. Trokhymchuk, *et al*., J. Phys. Chem. B **102**, 3012 (1998).
[53] L. Sarkisov and P.A. Monson, Phys. Rev. E **61**, 7231 (2000).
[54] J.K. Singh and D.A. Kofke, J. Chem. Phys. **121**, 9574 (2004).
[55] J.K. Singh and D.A. Kofke, Mol. Sim. **30**, 343 (2004).
[56] J.R. Errington, J. Chem. Phys. **118**, 9915 (2003).
[57] B.A. Berg and T. Neuhaus, Phys. Rev. Lett. **61**, 9 (1992).
[58] L.J. Van Poolen, C.D. Holcomb, and V.G. Niesen, Fluid Phase Equil. **129**, 105 (1997).
[59] S. Wierzchowski and D.A. Kofke, J. Chem. Phys. **114**, 8752 (2001).
[60] S. Bhattacharya and K.E. Gubbins, Langmuir **22**, 7726 (2006).
[61] R.L.C. Vink, K. Binder, and H. Lowen, Phys. Rev. Lett. **97**, 230603 (2006).
[62] J.K. Singh, D.A. Kofke, and J.R. Errington, J. Chem. Phys. **119**, 3405 (2003).
[63] H.L. Vortler, Collect. Czech. Chem. Commun. **73**, 518 (2008).
[64] K. Binder, Phys. Rev. A **25**, 1699 (1982).
[65] V. DE Grandis, P. Gallo, and M. Rovere, Europhys. Lett. **75**, 901 (2006).